NANO LETTERS

Letter

pubs.acs.org/NanoLett

Fluorescent Nanowire Heterostructures as a Versatile Tool for Biology Applications

Karl Adolfsson,[†] Henrik Persson,[†] Jesper Wallentin,[†] Stina Oredsson,[‡] Lars Samuelson,[†] Jonas O. Tegenfeldt,[†] Magnus T. Borgström,[†] and Christelle N. Prinz*[,†,§]

[†]Division of Solid State Physics—The Nanometer Structure Consortium, Lund University, 22100 Lund, Sweden

[‡]Department of Biology, Lund University, 22362 Lund, Sweden

[§]Neuronano Research Center, Lund University, 22100 Lund, Sweden

Supporting Information

ABSTRACT: Nanowires are increasingly used in biology, as sensors, as injection devices, and as model systems for toxicity studies. Currently, in situ visualization of nanowires in biological media is done using organic dyes, which are prone to photobleaching, or using microscopy methods which either yield poor resolution or require a sophisticated setup. Here we show that inherently fluorescent nanowire axial heterostructures can be used to localize and identify nanowires in cells and tissue. By synthesizing GaP−GaInP nanowire heterostructures, with nonfluorescent GaP segments and fluorescent GaInP segments, we created a barcode labeling system enabling the distinction of the nanowire morphological and chemical properties using fluorescence microscopy. The GaInP photoluminescence stability, combined with the fact that the nanowires can be coated with different materials while retaining their fluorescence, make these nanowires promising tools for biological and nanotoxicological studies.

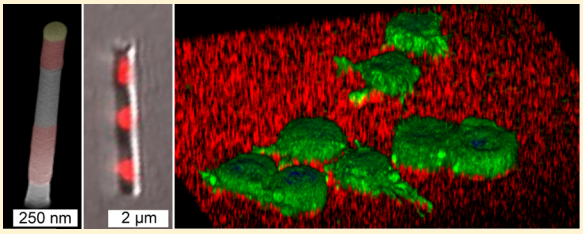

KEYWORDS: *Nanowires, fluorescence, photoluminescence, photobleaching, cells, toxicology*

Nanowires are promising tools for widespread use in biology, both for in vitro and in vivo applications. They have been demonstrated as powerful probes for cellular activity such as electrical signals,[1−5] enzymatic activity,[6] and exerted forces.[7,8] Nanowire arrays have been used to differentiate stem cells[9] and to promote neuronal growth[7,10−12] and can be used for cell transfection, either as solid substrates coated with biomolecules[13−16] or as nanoinjection devices.[17−20] The use of nanowires as biosensors has been demonstrated, with detection levels down to single molecules.[21−23] The high control over nanowire geometry makes them useful as a model system for high-aspect-ratio nanoparticles in toxicology.[24−26] Finally, nanowires have also been used for drug delivery, where they act as inorganic vectors enhancing the drug therapeutic effect.[27,28]

In most of these applications, the visualization of the nanowires is essential for interpreting the results. For instance, in the case of in vivo toxicity studies, assessing the nanowire distribution in tissues is crucial for the elucidation of the underlying interaction mechanisms. Similarly, when working with cell cultures, the determination of the position of the nanowires with respect to cells and cell components provides valuable information. For example, in the case of nanowire electrodes, it is necessary to determine which part of a neuron (axon, soma or dendrites) that has been recorded or stimulated. Moreover, when using nanowire-assisted transfection, the evaluation of the number of nanowires underneath a given cell is necessary for assessing the nanowire substrate-transfection efficiency. The identification and localization of nanowires in cells and tissues are currently achieved using different approaches, all of which have important limitations.

The cell cytosol can be loaded with a fluorescent organic molecule and imaged using confocal fluorescence microscopy.[14,29,30] Nanowires indenting the cytosol are then visualized by the absence of fluorescence and appear as dark rods. However, this method fails to visualize nanowires that do not indent the cell interior. Furthermore, the organic dyes in the cytosol are subject to photobleaching, which limits their use for long-term studies. The same holds true for nanowires labeled using organic fluorophores.[16,31] In addition, the latter method results in the modification of the nanowire surface, introducing a bias in the interaction of the nanowire with its surrounding. A third way to visualize nanowires consists of detecting laser light scattered off the nanowires, using laser scanning confocal microscopy.[25,26,29] In addition to the fact that this method offers poor image resolution, the substrate and surrounding tissue can also give rise to a strong reflected signal, which increases the difficulty of imaging the nanowires. Other methods include cell sectioning and subsequent scanning or transmission electron microscopy to visualize the interactions

Received: June 20, 2013
Revised: August 14, 2013
Published: August 28, 2013

   dx.doi.org/10.1021/nl4022754 | *Nano Lett.* 2013, 13, 4728−4732

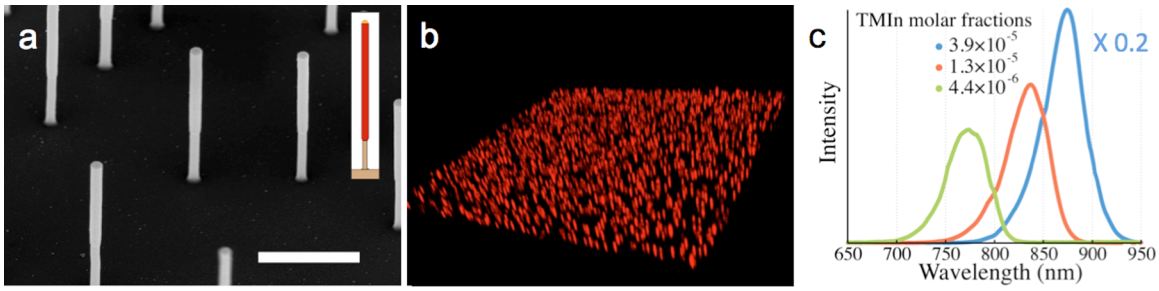

Figure 1. (a) Scanning electron micrograph of vertical GaP−GaInP nanowires on a GaP substrate (coated with 10 nm of gold−palladium to minimize charging effects). The GaInP segment is slightly thicker. Stage tilt 30°. Scale bar 1 μm. Inset: schematic drawing of nanowires (brown: GaP, red: GaInP, yellow: gold seed particle). (b) 3D reconstruction of confocal fluorescence *z*-stack images of 3 μm long GaP-GaInP nanowires standing as grown on a GaP substrate (50 μm × 50 μm). (c) Micro-PL emission spectra as a function of the TMIn molar fraction, demonstrating control of the emission wavelength. The intensity of the signal from the nanowire grown with highest TMIn content (blue) was cut by a factor of 5 in part c to fit into the graph.

of nanowires with subcellular components.[14,32−34] These methods are time-consuming, costly, and especially challenging when it comes to combining electron microscopy imaging with fluorescence microscopy on the exact same cell. Furthermore, in the case of epitaxial nanowires on a substrate, the use of standard sectioning methods such as microtomes is made impractical by the limited capability of the microtomes to cut the sample without shattering the crystalline substrate, thereby disrupting the tissue above it. Silicon nanowires have been imaged in vitro and in vivo using four-wave mixing and third-harmonic generation signals,[35] but this method requires a specialized experimental setup.

In this Letter, we show how the limitations described above can be overcome by using inherently fluorescent nanowire heterostructures. We report how gallium phosphide−gallium indium phosphide (GaP−GaInP) axial nanowire heterostructures can be used as fluorescent tools to visualize and identify individual nanowires in situ using confocal fluorescence microscopy. The nanowires were synthetized using the vapor−liquid−solid growth process and consist of GaP segments, which are nonfluorescent due to the indirect band gap, and direct band gap GaInP segments, where recombination over the band gap yields a strong fluorescence (photoluminescence). The fluorescence of the nanowires enables the precise determination of their location with respect to cell components and allows for long-term studies due to their inherent crystallinity leading to negligible photobleaching. By switching the indium reactant on and off during growth, we synthesized fluorescent barcode nanowires and demonstrated that they can be used for designed experiments where the morphological and optical properties of the nanowires are decoupled. We show two specific examples where nanowire barcodes can be used to distinguish nanowires that are otherwise indistinguishable using optical microscopy, in vitro and in vivo: nanowires with different diameters inside cells, and nanowires with different surface chemistries in the gut of the fruit fly *Drosophila melanogaster*.

Semiconductor nanowires allow for an almost unlimited combination of heterostructures, both in the axial and the radial (core−shell) growth direction.[36−40] The ternary semiconductor $Ga_xIn_{1-x}P$ has a direct bandgap emission, which is tunable from 925 nm (1.34 eV, for pure InP) down to about 560 nm (2.2 eV, where the bandgap becomes indirect).[41] Our group has previously demonstrated GaInP nanowires with tunable bandgap and corresponding tunable emission.[42,43] $Ga_xIn_{1-x}P$ nanowires were synthesized in a standard commercial metal organic vapor phase epitaxy (MOVPE) reactor at 440 °C (Aixtron 200/4) from gold catalytic nanoparticles (see Supporting Information and Table S1 for a detailed experimental protocol). Briefly, a GaP spacer was grown using trimethylgallium (TMGa) as a gas precursor and a GaInP segment was grown by introducing trimethylindium (TMIn) to the flow. HCl was used to prevent unintended radial growth throughout the growth.[44]

The resulting nanowires are shown in Figure 1. They exhibit strong fluorescence and can be imaged in three dimensions on the substrate using confocal microscopy (LSM 510, Carl Zeiss SMT GmbH). The GaP substrate and the GaP nanowire segments do not give any significant signal. The emission spectrum of the GaInP segment was determined using microphotoluminescence (Micro-PL) at room temperature using an excitation wavelength of 532 nm. The emission peak is strongly dependent on the TMIn molar fraction during growth (Figure 1c). In line with our previous work, increasing the TMIn molar fraction increases the In fraction, $1 - x$, in the $Ga_xIn_{1-x}P$ segments, which reduces the bandgap and increases the wavelength of the emitted light.[42] The PL signal was significantly higher for nanowires grown with high TMIn molar fraction. Unless otherwise noted, all GaInP segments in this paper were synthesized using a TMIn molar fraction of 1.3×10^{-5}, which corresponds to an emission peak wavelength of 830 nm.

Using Micro-PL measurements with a laser excitation intensity of 200 W/cm^2, we estimated the emission rate of a single GaP-GaInP nanowire to 3.4×10^9 photons per second (see the Supporting Information for detailed experimental protocol and calculation). Assuming a 1% photon detection efficiency, this means that the nanowires can be imaged using a 1.0 NA-objective at a standard 30 frames per second acquisition speed with an expected location determination uncertainty of $\sigma = \lambda/(\mathrm{NA}\sqrt{n}) = 0.75$ nm[31,45,46] (where λ is the emission wavelength, NA is the objective numerical aperture, and n the number of detected photons).

To examine whether GaP−GaInP nanowires could be used for localization of nanowires within cells, we cultured L929 fibroblasts on a substrate with GaP-GaInP nanowires. Cells were fixed, DNA and actin were labeled using bisbenzimide, and FITC-conjugated phalloidin, respectively (see the Supporting Information for detailed experimental protocol). The samples were imaged using laser scanning confocal microscopy. Individual nanowires are clearly visible as red dots in the top-view 2D image and as rods in the projection along the *z*-axis

dx.doi.org/10.1021/nl4022754 | *Nano Lett.* 2013, 13, 4728−4732

(Figure 2). The GaInP-segment fluorescence enables the precise determination of the nanowire position with respect

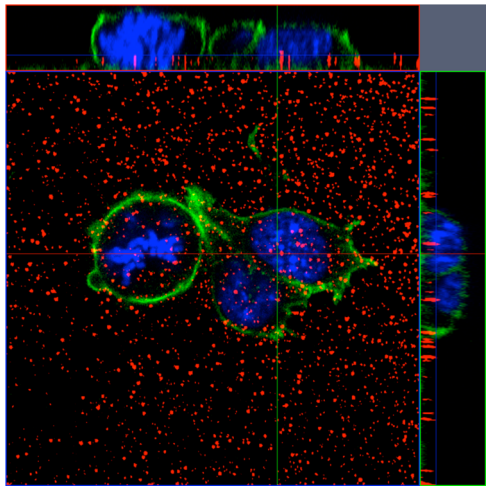

Figure 2. Confocal fluorescence image (72 μm × 72 μm × 11 μm) of L929 mouse fibroblasts cultured on 2.5 μm long GaP−GaInP nanowires (blue: DNA; green: actin filaments; red: nanowires). Side panels show the projection along the *z*-axis. The GaInP segment fluorescence enables the precise determination of the nanowire position with respect to cell structures.

to cell components. On the top view, the leftmost cell is in metaphase with chromosomes aligned. The cell is clearly rolled up in preparation for cell division. Some nanowires are colocalized with the chromosomal DNA. In the side panels, nanowires can be seen indenting the cell nuclei.

To compare the GaInP fluorescence stability with traditional dyes, we acquired time-lapse images of cells labeled with organic fluorescent dyes and cultured on GaP−GaInP nanowires. In these experiments, the cell nuclei were stained with bisbenzimide, and the actin filaments were labeled using FITC-conjugated phalloidin (see Supporting Information for detailed experimental protocol). The blue (bisbenzimide), green (FITC), and red (GaInP) fluorescence signals were detected in separate confocal photomultiplier detectors using sequential excitations of 405 nm (for bisbenzimide fluorescence detection) and 488 nm (for nanowire and FITC fluorescence detection) of constant intensity. Each detector count was measured as a function of the frame number and normalized to the initial count. It should be noted that the GaInP segments are excitable by both 405 and 488 nm lasers, due to their broad excitation spectrum and therefore have been subjected to twice as frequent excitations compared to FITC and bisbenzimide during this experiment. Despite this, we observed much less photobleaching of the GaInP compared to bisbenzimide and FITC (see Figure 3), which makes the nanowires particularly suitable for time-lapse microscopy and nanotoxicological studies. Note that these nanowires were not protected by any coatings.

As a proof of principle that GaP−GaInP heterostructures can be used for identifying nanowires in a similar way as in barcode identification systems, in vitro and in vivo, we performed two sets of experiments as laid out below, for different sizes of nanowires and for nanowires with different surface treatments.

To distinguish between nanowires of similar lengths but different diameters, we synthesized 40 nm diameter nanowires with a single fluorescent segment (GaP−GaInP) and 80 nm

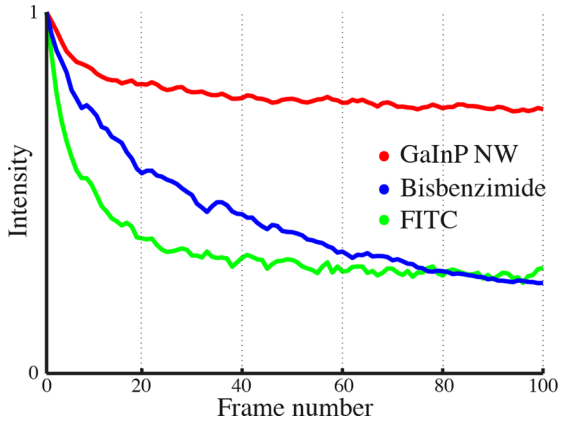

Figure 3. Photostability of GaInP compared to bisbenzimide and FITC for sequential confocal scans. Relative intensity of bisbenzimide-labeled cellular DNA (blue), FITC-phalloidin-labeled actin filaments (green), and GaInP nanowires (red) as a function of confocal frame number (each frame consisting of two sequential scans, one with 405 nm and one with a 488 nm excitation wavelength). The nanowires are less prone to photobleaching compared to bisbenzimide and FITC. In each case, the signal has been normalized to the value measured in the initial frame.

diameter nanowires with two fluorescent segments (GaP−GaInP−GaP−GaInP) (Figure 4) and added them to a cell culture (see Supporting Information for a detailed experimental protocol).

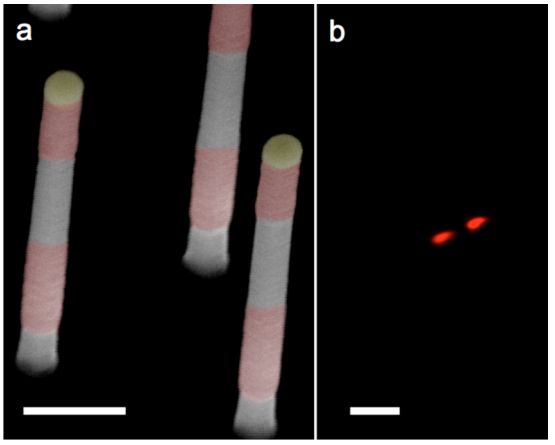

Figure 4. (a) False color SEM image of GaP-GaInP dual fluorescent segment barcode nanowires (red: GaInP; gray: GaP; yellow: gold seed particle). Stage tilt 30°. Scale bar 250 nm. (b) Confocal fluorescence top view image of one GaP−GaInP barcode nanowire lying on a glass coverslip. Scale bar 2 μm.

A confocal image of a fibroblast having phagocytized one 40 nm and one 80 nm nanowire can be seen in Figure 5a. Despite the subwavelength diameter of the nanowires, they can easily be distinguished based on the number of axial fluorescent segments.

To distinguish between nanowires of similar dimensions but having different surface chemistries in vivo using the barcode system, we synthesized a single GaInP segment and dual GaInP segment nanowires of identical length and diameter. We coated the single-segment nanowires with HfO_x and the dual-segment nanowires with AlO_x using atomic layer deposition (ALD, see Supporting Information for a detailed experimental protocol

dx.doi.org/10.1021/nl4022754 | *Nano Lett.* 2013, 13, 4728−4732

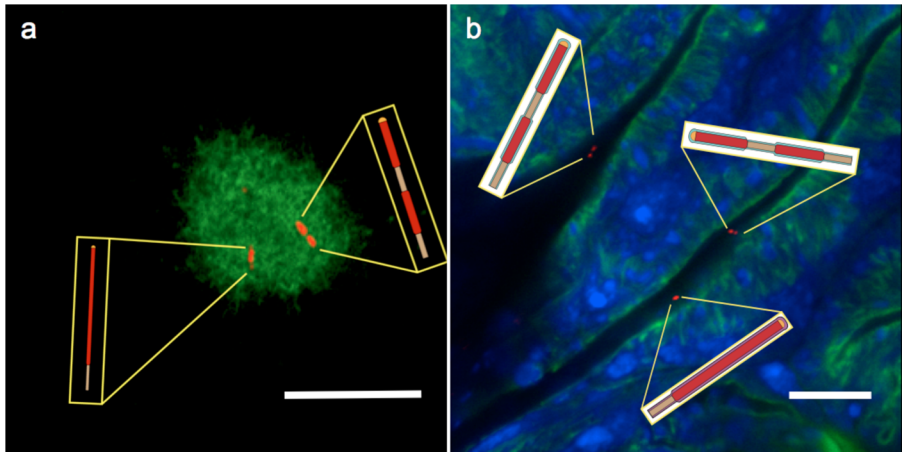

Figure 5. Barcode nanowires as diameter/morphology and surface-chemistry identification tools. (a) Confocal microscopy image of a L929 fibroblast that has internalized a 40 nm diameter (single fluorescent segment) and a 80 nm diameter (two fluorescent segments) nanowire of identical length. (b) Confocal microscopy image of HfO_x-coated nanowires (single fluorescent segment) and AlO_x-coated nanowires (two fluorescent segments) in the Drosophila gut. Scale bars 10 μm.

and Figure S1 for fluorescence spectra after coating). The nanowires were suspended in PBS with 15% sucrose and given to Drosophila flies as sole source of food and water for 24 h. The guts were stained for cell nuclei and actin filaments and examined using confocal microscopy. Single and dual segment nanowires are clearly identifiable in the Drosophila gut (see Figure 5b).

The ability to distinctly label nanowires that would otherwise be indistinguishable using optical microscopy offers great advantages. Cell or tissue internalization and distribution of different nanowires can be investigated simultaneously for a large range of nanowire types in the same cell or tissue, reducing the number of necessary experiments. It also enables the administration of nanowires at different time points or using different administration routes while comparing the effects of the different exposure patterns. Moreover, the feasibility of assessing the distribution of nanowires by simple optical microscopy makes the method versatile with respect to color multiplexing and significantly more time and cost-effective compared to conventional SEM/TEM imaging.

To further demonstrate that GaP−GaInP nanowires can be used as a barcode labeling system, we synthesized three fluorescent segment nanowires, as well as dual segment nanowires containing both a long and a short fluorescent segment (see Supporting Information and Table S1 for detailed experimental protocol and dimensions). The nanowires were detached from the GaP substrate, deposited on a glass coverslip, and imaged using confocal microscopy. The three segments (Figure 6a,c) as well as the long and short segments (Figure 6b,d) are clearly identifiable in the images. We estimated the minimum distance between GaInP segments for which they can be distinctly identified to approximately 200 nm (see Figure S2). Hence, this system can offer a high number of pattern combinations, which can be used to optically label multiple nanowire properties in the same experiment.

In summary, we demonstrated that GaP-GaInP nanowire axial heterostructures can be used for localization and identification of nanowires in living cells and tissues. We realized a barcode labeling scheme by insertion of GaInP segments into GaP nanowires and showed how it can be used as a nanowire identification tool to distinguish between nanowires of identical lengths but different diameters as well as nanowires of identical dimensions but different surface chemistries. The strong and stable GaInP photoluminescence opens up for ultraprecise localization of the nanowires, which is important for detailed understanding of the nanowire-cell/tissue interactions on the subcellular level with strong technical relevance for the use of nanowires in biology, specifically in fields such as cell mechanics, nanotoxicology, stem cell biology, systems biology, and oncology.

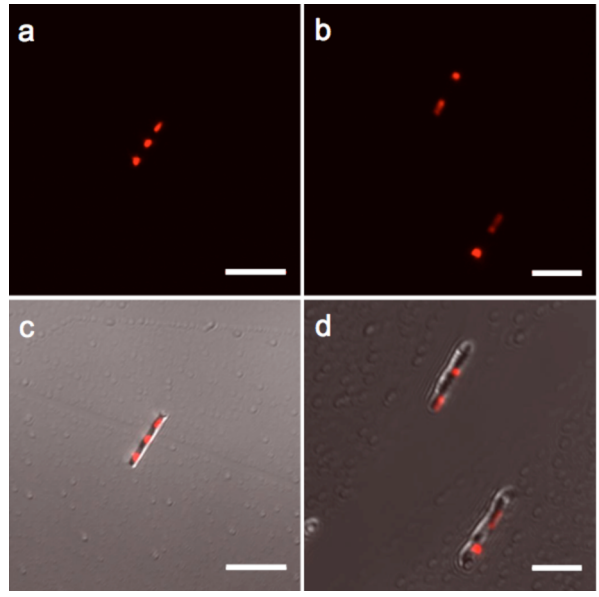

Figure 6. Fluorescent nanowire barcodes. Confocal images of a nanowire with three fluorescent segments (a, c) and two nanowires with both a long and a short GaInP segment (b, d). The top panels show the fluorescence images, and the bottom panels are composites of fluorescence and laser-reflection images. Scale bars: 5 μm (a, c) and 3 μm (b, d).

■ ASSOCIATED CONTENT

Supporting Information

Detailed experimental protocols, microPL measurements after nanowire coating, GaInP emission−rate calculation, and the determination of the fluorescent segment spatial resolution.

dx.doi.org/10.1021/nl4022754 | Nano Lett. 2013, 13, 4728−4732

This material is available free of charge via the Internet at http://pubs.acs.org.

AUTHOR INFORMATION

Corresponding Author

*E-mail: christelle.prinz@ftf.lth.se.

Author Contributions

K.A. and H.P. contributed equally to this work.

Notes

The authors declare no competing financial interest.

ACKNOWLEDGMENTS

This work was supported by nmC@LU, the Swedish Foundation for Strategic Research (SSF), the Swedish Research Council (VR), the Neuronano Research Center in Lund, the Crafoord Foundation, the Carl Tryggers foundation and the Knut and Alice Wallenberg Foundation. We thank Prof. Udo Häcker from the Department of Experimental Medical Science at Lund University for giving us access to his laboratory for the Drosophila experiments.

REFERENCES

(1) Robinson, J. T.; Jorgolli, M.; Shalek, A. K.; Yoon, M. H.; Gertner, R. S.; Park, H. *Nat. Nanotechnol.* **2012**, *7*, 180−184.

(2) Suyatin, D. B.; Wallman, L.; Thelin, J.; Prinz, C. N.; Jorntell, H.; Samuelson, L.; Montelius, L.; Schouenborg, J. *PLoS One* **2013**, *8*, e56673.

(3) Xie, C.; Lin, Z. L.; Hanson, L.; Cui, Y.; Cui, B. X. *Nat. Nanotechnol.* **2012**, *7*, 185−190.

(4) Duan, X. J.; Gao, R. X.; Xie, P.; Cohen-Karni, T.; Qing, Q.; Choe, H. S.; Tian, B. Z.; Jiang, X. C.; Lieber, C. M. *Nat. Nanotechnol.* **2012**, *7*, 174−179.

(5) Jiang, Z.; Qing, Q.; Xie, P.; Gao, R. X.; Lieber, C. M. *Nano Lett.* **2012**, *12*, 1711−1716.

(6) Na, Y. R.; Kim, S. Y.; Gaublomme, J. T.; Shalek, A. K.; Jorgolli, M.; Park, H.; Yang, E. G. *Nano Lett.* **2013**, *13*, 153−158.

(7) Hallstrom, W.; Martensson, T.; Prinz, C.; Gustavsson, P.; Montelius, L.; Samuelson, L.; Kanje, M. *Nano Lett.* **2007**, *7*, 2960−2965.

(8) Li, Z.; Song, J. H.; Mantini, G.; Lu, M. Y.; Fang, H.; Falconi, C.; Chen, L. J.; Wang, Z. L. *Nano Lett.* **2009**, *9*, 3575−3580.

(9) Bucaro, M. A.; Vasquez, Y.; Hatton, B. D.; Aizenberg, J. *ACS Nano* **2012**, *6*, 6222−6230.

(10) Hallstrom, W.; Prinz, C. N.; Suyatin, D.; Samuelson, L.; Montelius, L.; Kanje, M. *Langmuir* **2009**, *25*, 4343−4346.

(11) Piret, G.; Perez, M. T.; Prinz, C. N. *Biomaterials* **2013**, *34*, 875−887.

(12) Prinz, C.; Hallstrom, W.; Martensson, T.; Samuelson, L.; Montelius, L.; Kanje, M. *Nanotechnology* **2008**, *19*, 345101.

(13) Kim, W.; Ng, J. K.; Kunitake, M. E.; Conklin, B. R.; Yang, P. D. *J. Am. Chem. Soc.* **2007**, *129*, 7228−7229.

(14) Mumm, F.; Beckwith, K. M.; Bonde, S.; Martinez, K. L.; Sikorski, P. *Small* **2013**, *9*, 263−272.

(15) Shalek, A. K.; Gaublomme, J. T.; Wang, L. L.; Yosef, N.; Chevrier, N.; Andersen, M. S.; Robinson, J. T.; Pochet, N.; Neuberg, D.; Gertner, R. S.; Amit, I.; Brown, J. R.; Hacohen, N.; Regev, A.; Wu, C. J.; Park, H. *Nano Lett.* **2012**, *12*, 6498−6504.

(16) Shalek, A. K.; Robinson, J. T.; Karp, E. S.; Lee, J. S.; Ahn, D.-R.; Yoon, M.-H.; Sutton, A.; Jorgolli, M.; Gertner, R. S.; Gujral, T. S.; MacBeath, G.; Yang, E. G.; Park, H. *Proc. Natl. Acad. Sci. U.S.A.* **2010**, *107*, 1870−1875.

(17) Peer, E.; Artzy-Schnirman, A.; Gepstein, L.; Sivan, U. *ACS Nano* **2012**, *6*, 4940−4946.

(18) Persson, H.; Beech, J. P.; Samuelson, L.; Oredsson, S.; Prinz, C. N.; Tegenfeldt, J. O. *Nano Res.* **2012**, *5*, 190−198.

(19) Skold, N.; Hallstrom, W.; Persson, H.; Montelius, L.; Kanje, M.; Samuelson, L.; Prinz, C. N.; Tegenfeldt, J. O. *Nanotechnology* **2010**, *21*, 155301.

(20) VanDersarl, J. J.; Xu, A. M.; Melosh, N. A. *Nano Lett.* **2012**, *12*, 3881−3886.

(21) Patolsky, F.; Zheng, G. F.; Hayden, O.; Lakadamyali, M.; Zhuang, X. W.; Lieber, C. M. *Proc. Natl. Acad. Sci. U.S.A.* **2004**, *101*, 14017−14022.

(22) Zheng, G. F.; Gao, X. P. A.; Lieber, C. M. *Nano Lett.* **2010**, *10*, 3179−3183.

(23) Zheng, G. F.; Patolsky, F.; Cui, Y.; Wang, W. U.; Lieber, C. M. *Nat. Biotechnol.* **2005**, *23*, 1294−1301.

(24) Schinwald, A.; Murphy, F. A.; Prina-Mello, A.; Poland, C. A.; Byrne, F.; Movia, D.; Glass, J. R.; Dickerson, J. C.; Schultz, D. A.; Jeffree, C. E.; MacNee, W.; Donaldson, K. *Toxicol. Sci.* **2012**, *128*, 461−470.

(25) Linsmeier, C. E.; Prinz, C. N.; Pettersson, L. M. E.; Caroff, P.; Samuelson, L.; Schouenborg, J.; Montelius, L.; Danielsen, N. *Nano Lett.* **2009**, *9*, 4184−4190.

(26) Adolfsson, K.; Schneider, M.; Hammarin, G.; Hacker, U.; Prinz, C. N. *Nanotechnology* **2013**, *24*, 285101.

(27) Peng, F.; Su, Y. Y.; Wei, X. P.; Lu, Y. M.; Zhou, Y. F.; Zhong, Y. L.; Lee, S. T.; He, Y. *Angew. Chem., Int. Ed.* **2013**, *52*, 1457−1461.

(28) Tian, Z. R.; Sharma, A.; Nozari, A.; Subramaniam, R.; Lundstedt, T.; Sharma, H. S. *CNS Neurol. Disorders* **2012**, *11*, 86−95.

(29) Berthing, T.; Bonde, S.; Sorensen, C. B.; Utko, P.; Nygard, J.; Martinez, K. L. *Small* **2011**, *7*, 640−647.

(30) Berthing, T.; Bonde, S.; Rostgaard, K. R.; Madsen, M. H.; Sorensen, C. B.; Nygard, J.; Martinez, K. L. *Nanotechnology* **2012**, *23*, 415102.

(31) Hallstrom, W.; Lexholm, M.; Suyatin, D. B.; Hammarin, G.; Hessman, D.; Samuelson, L.; Montelius, L.; Kanje, M.; Prinz, C. N. *Nano Lett.* **2010**, *10*, 782−787.

(32) Hanson, L.; Lin, Z. C.; Xie, C.; Cui, Y.; Cui, B. X. *Nano Lett.* **2012**, *12*, 5815−5820.

(33) Persson, H.; Kobler, C.; Molhave, K.; Samuelson, L.; Tegenfeldt, J. O.; Oredsson, S.; Prinz, C. N. *Small* **2013**, No. 10.1002/smll.201300644.

(34) Wierzbicki, R.; Kobler, C.; Jensen, M. R. B.; lopacinska, J.; Schmidt, M. S.; Skolimowski, M.; Abeille, F.; Qvortrup, K.; Molhave, K. *Plos One* **2013**, *8*, e53307.

(35) Jung, Y.; Tong, L.; Tanaudommongkon, A.; Cheng, J. X.; Yang, C. *Nano Lett.* **2009**, *9*, 2440−2444.

(36) Bjork, M. T.; Ohlsson, B. J.; Sass, T.; Persson, A. I.; Thelander, C.; Magnusson, M. H.; Deppert, K.; Wallenberg, L. R.; Samuelson, L. *Nano Lett.* **2002**, *2*, 87−89.

(37) Gudiksen, M. S.; Lauhon, L. J.; Wang, J.; Smith, D. C.; Lieber, C. M. *Nature* **2002**, *415*, 617−620.

(38) Lauhon, L. J.; Gudiksen, M. S.; Lieber, C. M. *Philos. Trans. R. Soc. London, Ser. A* **2004**, *362*, 1247−1260.

(39) Lauhon, L. J.; Gudiksen, M. S.; Wang, C. L.; Lieber, C. M. *Nature* **2002**, *420*, 57−61.

(40) Wu, Y. Y.; Fan, R.; Yang, P. D. *Nano Lett.* **2002**, *2*, 83−86.

(41) Wadehra, A.; Nicklas, J. W.; Wilkins, J. W. *Appl. Phys. Lett.* **2010**, *97*, 092119.

(42) Jacobsson, D.; Persson, J. M.; Kriegner, D.; Etzelstorfer, T.; Wallentin, J.; Wagner, J. B.; Stangl, J.; Samuelson, L.; Deppert, K.; Borgstrom, M. T. *Nanotechnology* **2012**, *23*, 245601.

(43) Wallentin, J.; Poncela, L. B.; Jansson, A. M.; Mergenthaler, K.; Ek, M.; Jacobsson, D.; Wallenberg, L. R.; Deppert, K.; Samuelson, L.; Hessman, D.; Borgstrom, M. T. *Appl. Phys. Lett.* **2012**, *100*, 251103.

(44) Borgstrom, M. T.; Wallentin, J.; Tragardh, J.; Ramvall, P.; Ek, M.; Wallenberg, L. R.; Samuelson, L.; Deppert, K. *Nano Res.* **2010**, *3*, 264−270.

(45) Thompson, R. E.; Larson, D. R.; Webb, W. W. *Biophys. J.* **2002**, *82*, 2775−2783.

(46) Yildiz, A.; Forkey, J. N.; McKinney, S. A.; Ha, T.; Goldman, Y. E.; Selvin, P. R. *Science* **2003**, *300*, 2061−2065.